Journal of Physics: Conference Series **190** (2009) 012140 doi:10.1088/1742-6596/190/1/012140

Formation and reactivity of Cr^{II} carbonyls hosted in polar and non polar supports

D Gianolio[1], E. Groppo[1], J. Estephane[2], C. Prestipino[3], S. Nikitenko[4], A. Zecchina[1], S. Bordiga[1], M. Taoufik[2], E. A. Quadrelli[2], J. M. Basset[2], C. Lamberti[1]

[1]Department of Inorganic, Physical and Materials Chemistry, NIS Centre of Excellence and INSTM Center, University of Turin, Turin, Italy;
[2]Laboratoire de ChimieOrganometallique de Surface, UMR5265 "LC2P2", CNRS UCBL1 CPE, Villeurbanne Cedex, France;
[3]ESRF, Grenoble Cedex, France; present address Rennes-1 University, France;
[4]Netherlands Organization for Scientific Research (NWO), DUBBLE @ESRF, Grenoble Cedex, France

gianolio@studenti.ph.unito.it

Abstract. Organometallic complexes hosted inside porous frameworks are particularly interesting because of possible application in heterogeneous catalysis or electronic devices and optical materials. We present here a detailed spectroscopic investigation on the structure and reactivity towards simple reagents (such as CO) of chromocene molecules (Cp_2Cr) encapsulated into the nanovoids of two different matrices: a non polar polystyrene (PS) and a polar NaY zeolite. We demonstrate that stable $Cp_2Cr(CO)$ complexes are formed in PS, while in NaY the presence of high internal electric fields confers to the Cp_2Cr molecules a much higher reactivity towards CO. In situ EXAFS data, combined with other spectroscopic techniques and ab initio theoretical calculations, allowed the structural determination of the reaction products and afforded the full comprehension of the complex reactivity of Cp_2Cr molecules inside the cavities of PS and NaY hosts.

1. Introduction

In the last decades many efforts were devoted to find new methods for metal incorporation and catalyst immobilization inside nanoporous scaffolds. In particular, the inclusion of organometallic complexes inside host frameworks gives the possibility of several applications such as electronic devices, optical materials or heterogeneous catalysis.[1-7] Metallocenes are organometallic substrates of interest to investigate potential reactivity enhancement; among them, chromocene (Cp_2Cr) is a challenging candidate, both for applicative (being precursor of the well known Union Carbide olefin catalyst[8]) and for theoretical reasons (because the modeling of open shell systems is still a challenge).[9-13] The experimental approaches adopted so far to investigate the properties and the reactivity of these systems (such as matrix isolation technique[14] and dissolution in a solvent[15,16]), suffered of some disadvantages. Among the major problems we cite the air sensitivity of Cp_2Cr (that forced us to work in controlled atmosphere) and its tendency to form clusters (so that most of the techniques give information about the clusters and not about the isolated molecules).

In this work new strategies were developed in order to obtain spectroscopic information on isolated Cp_2Cr molecules and on their reactivity, in particular towards CO. Two matrices were adopted as "scaffolds" to encapsulate and isolate molecules in their cavities (see Figure 1): (i) a non polar nanoporous polystyrene matrix (in the following PS);[17] and (ii) a polar NaY zeolite,[18] that is expected to enhance the reactivity of the hosted molecules by means of the internal electrostatic fields. In fact zeolitic voids would function as "nanoscale reaction chambers", where the reactivity of guest organometallic complexes can provide molecular insights into the elementary steps of heterogeneous catalysis.[1] This strategy allowed us to determine, by means of in situ IR and XAFS experiments, the vibrational and structural features of isolated Cp_2Cr molecules and to follow in situ their reactivity towards CO.

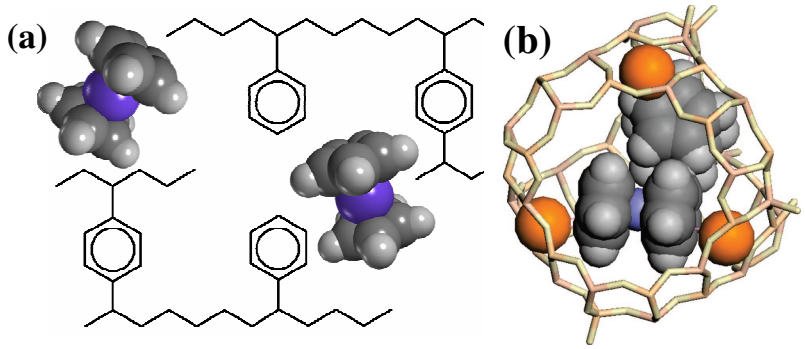

Figure 1. Cp_2Cr molecules encapsulated inside a 2D portion of PS matrix (part a) and a 3D portion of a zeolite cell (part b) where framework atoms are represented in the stick mode (Si and Al, light orange; O, light yellow) and Na^+ cations as orange CPK spheres

2. Experimental Section

Sample preparation. Cp_2Cr (Strem Chemicals, purified) was directly sublimed inside the hosting matrixes, previously outgassed in order to remove physisorbed water (at RT and 450°C for PS and NaY, respectively). The final Cr loading, evaluated a posteriori from the edge-jump of the extended X-ray absorption fine structure (EXAFS) signal in transmission mode, was around 1 wt % in both cases. This makes negligible self-absorption phenomena in fluorescence XAFS. Because Cp_2Cr is highly air sensitive, all the experiments were conducted in controlled atmosphere. FTIR experiments were conducted on samples in the form of self supporting pellets inside a cell allowing in situ treatment and measurements, on a Bruker IFS66 instrument at a resolution of 2 cm^{-1}. For XAFS measurements, the samples were stored inside capillaries of 1 mm in diameter, filled in the glove box, and sealed in presence or absence of CO.

XAFS measurements and data analysis. EXAFS measurements were performed at BM26A (ESRF, Grenobl) at the Cr K-edge (5989 eV). The white beam was monochromatized using a Si(111) double crystal; harmonic rejection was performed by using a meridionally focusing mirror with an angle of incidence of 2.8 mrad and either a platinum or silicon coating. Due to Cp_2Cr dilution and the thickness of the sample (defined by the diameter of the capillary), EXAFS spectra were collected in fluorescence mode, by means of a 9 elements germanium monolithic detector positioned at almost 90° with respect to the direction of the X-ray beam (45° with respect to the capillary). Ionization chambers were filled with 1 bar of 20% N_2 – 80% He. While measuring inside sealed capillaries, the well-established procedure adopted for X-ray powder diffraction (XRPD) experiments was followed. Low temperature experiments were conducted by using a cryostream blowing a liquid nitrogen jet coaxial to the capillary. The beam was vertically focused in order to reach a dimension on the sample of 0.3 mm. The horizontal slits were optimized to fit with the interval of uniform filling of the capillary. XANES part of the spectra have been acquired with an energy step of 0.4 eV and an integration time of 2 s/point. EXAFS part of the spectra were collected up to 12 $Å^{-1}$ with a variable sampling step in energy, resulting in $\Delta k = 0.05$ $Å^{-1}$, and an integration time that linearly increases with k from 5 to 20 s/point to account for the low signal-to-noise ratio at high k values. For each sample, three equivalent EXAFS spectra were acquired and averaged before the data analysis.

EXAFS data analysis has been performed using the Arthemis software.[19] Phase and amplitudes have been calculated by FEFF6 code[20] using as input the structures optimized by ab initio calculations.[17] Phase and amplitudes have been successfully checked with the experimental signal obtained by Cp_2Cr in toluene solution. For each sample, the averaged $k^3\chi(k)$ functions were Fourier transformed in the Δk = 2.0-10.0 Å^{-1} interval, because at higher k value the signal to noise ratio was too low. The fits were performed in R-space in the ΔR = 1.0-4.5 Å range. In the EXAFS data analysis of the Cp_2Cr molecule, we have considered the signals due to 10 Cr-C single scattering paths, and to several triangular multiple scattering paths, involving two C atoms belonging to the same Cp ring. Conversely, collinear and triangular multiple scattering paths involving two C atoms of the two different Cp rings do not contribute as expected. This fact, already evidenced by Natoli et al.[21] for the $FeCp_2$ molecule, is explained by considering the dynamic equilibrium between staggered and eclipsed configurations favored by the very low barrier to internal rotations around the C_5 axis. To limit the number of optimized parameters, the two Cp rings have been considered as rigid units, whose distance from Cr is allowed to change in a symmetric way. Using this parameter all path variations can be defined in a straightforward geometric way. For the $[Cp_2Cr(CO)]^+$ and $[CpCr(CO)_3]^-$ models, two additional parameters have been added: the Cr-CO distance and corresponding Debye-Waller factor, by considering the CO molecule as a rigid unit linearly bonded to Cr(II).

3. Results and Discussions

3.1. Structural Properties of Hosted Cp_2Cr

The k^3-weighted, phase-uncorrected Fourier transform (FT) of the EXAFS signals of Cp_2Cr hosted in both PS and NaY matrixes (black and blue curves in Figure 2, in both modulus and imaginary parts), are very similar to that of Cp_2Cr in toluene solutions (assumed as model for isolated molecules, grey curves in Figure 2). In fact they are dominated by a first-shell contribution around 1.6 Å, due to the Cr-C SS paths, whereas no contributions assignable to a Cr-Cr path characteristic for Cp_2Cr clusters are observed. Also the three XANES spectra exhibit basically the same features, confirming that the molecules are really isolated. A more complete study of the electronic properties and transitions is presented in a previous work.[18]

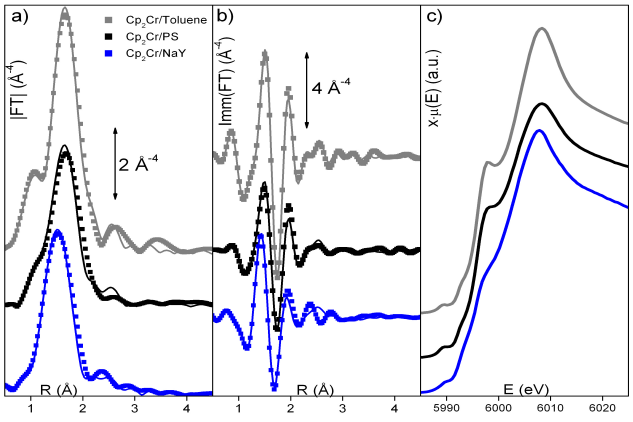

Figure 2. Modulus (a) and imaginary parts (b) of the k^3-weighted, phase-uncorrected FT of EXAFS signals for Cp_2Cr/toluene (grey curves), Cp_2Cr/PS (black curves), and Cp_2Cr/NaY (blue curves); experimental data (square dots) are overlapped to the best fits (full lines). Part (c) reports the corresponding XANES spectra.

A detailed analysis of the EXAFS data (Table 1) reveals that Cp_2Cr molecules hosted in PS retain the same geometry found in solution, whereas they are slightly distorted inside NaY: in particular, a shorter mean distance $\langle d_{Cr\text{-}C} \rangle$ is observed (resulting in a shift of the main peak in |FT| to shorter R values), accompanied by a higher value of σ^2 Debye-Waller factor, indicating a higher heterogeneity of species. This is assigned to different local electric fields experienced by Cp_2Cr molecules due to different statistical cation distribution in the zeolite supercages (Figure 1).

	Cp_2Cr/toluene	Cp_2Cr/PS	Cp_2Cr/NaY
S_0^2	0.7 ± 0.1	0.7	0.9 ± 0.1
ΔE_0 (eV)	0 ± 1	+1 ± 1	-4 ± 2
$<d_{Cr-C}>$ (Å)	2.169 ± 0.006	2.165 ± 0.008	2.11 ± 0.01
σ^2_{Cr-Cp} (Å^2)	0.003 ± 0.001	0.0070 ± 0.0005	0.010 ± 0.002
n° variables	4	3	4
R_{factor}	0.020	0.037	0.057

Table 1. Summary of the structural parameters optimized in the fit of the EXAFS data for the Cp_2Cr/toluene, Cp_2Cr/PS and Cp_2Cr/NaY systems. The fits run in the ΔR = 1.0-4.5 Å range.

3.2. Vibrational and Structural Properties of the Reaction Products of Hosted Cp_2Cr and CO

Interaction of CO with hosted Cp_2Cr/matrix system was firstly investigated by in situ IR spectroscopy. In the case of PS, a time-stable $Cp_2Cr(CO)$ monocarbonyl complex is formed, characterized by an intense ν(CO) band at 1900 cm^{-1} (Figure 3a),[17] very similar to that already reported in literature in the case of $Cp_2Cr(CO)$ in toluene solution.[15,16] Conversely, when the Cp_2Cr/NaY is contacted with CO, a rapid evolution in time is observed. An intense band in the ν(CO) region at 1850 cm^{-1} immediately appears (blue curve in Figure 3b), that is assigned to the $Cp_2Cr(CO)$ monocarbonyl complex. The red-shift of ν(CO) with respect to the value found in PS and reported in literature can be explained by the high ionicity of the NaY environment. By waiting in time this band is progressively eroded, and simultaneously three new bands at 1893, 1773 and 1724 cm^{-1} (red triangles in Figure 3b) appear, accompanied by a weak component at ~1980 cm^{-1} (red square) growing in a similar way. The evolution of the spectra suggests that the monocarbonyl precursor is transformed into a tricarbonyl charged species $[CpCr(CO)_3]^-$, through the loss of a Cp ring.[22] The weak component at ~1980 cm^{-1} can be assigned to a fraction of $[Cp_2Cr(CO)]^+$ species.[23,24]

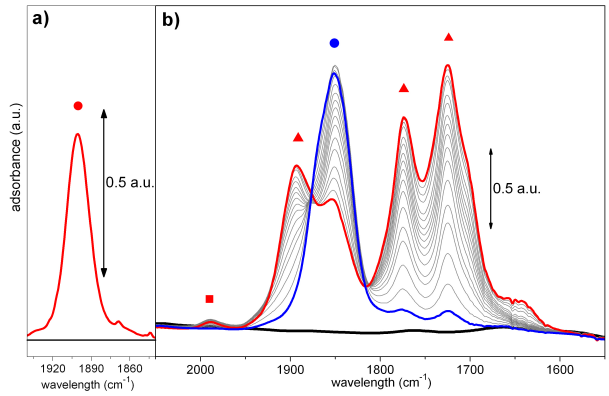

Figure 3. Time evolution of the FTIR spectra (at RT) of the Cp_2Cr/PS (part a) and Cp_2Cr/NaY systems (part b) before dosage of CO (black), immediately after (blue), and after 1h of exposure to CO (red).

The k^3-weighted FT of the EXAFS data and the corresponding XANES spectra (Figure 4a-d) reflect the behavior observed by IR and highlight the structural variations undergone by the Cp_2Cr molecule upon CO addition in the two matrices. In particular, for the Cp_2Cr/PS system, the |FT| (Figure 4a) exhibits an increase of the intensity of the first shell and a shift toward higher R values. The result of the data analysis (Table 2) prove the insertion of a CO ligand and the consequent rearrangement of the Cp rings, with elongation of the average $<d_{Cr-C}>$ distance. The additional component, centered around 2.5 Å, is ascribed to the strong collinear Cr-C-O MS contributions. In a similar way, the modification of all the pre-edge XANES features confirm that the Cp_2Cr molecules loose their symmetry and undergo a relevant distortion after interaction with CO. Coming to the Cp_2Cr/NaY system, because the time of CO contact in the XAS experiment is much longer than that of IR, the initial species $Cp_2Cr(CO)$ is not expected to be detected by this technique, while only the final state with the co-presence of the $[CpCr(CO)_3]^-$ and $[Cp_2Cr\text{-}(CO)]^+$ species is expected to be observed. Indeed, the XANES spectrum of Cp_2Cr/NaY system shows strong modification upon CO addition, suggesting a better molecular definition of the Cr species formed upon CO contact. The $[CpCr(CO)_3]^-$

and $[Cp_2Cr(CO)]^+$ product species hypothesized from the IR study could justify this behaviour. The two products should be characterized by a different formal oxidation state, but the position of the edge is almost unaltered; this can be explained by considering that the charges are delocalized across the entire molecule and not localized on the Cr centre.[18]

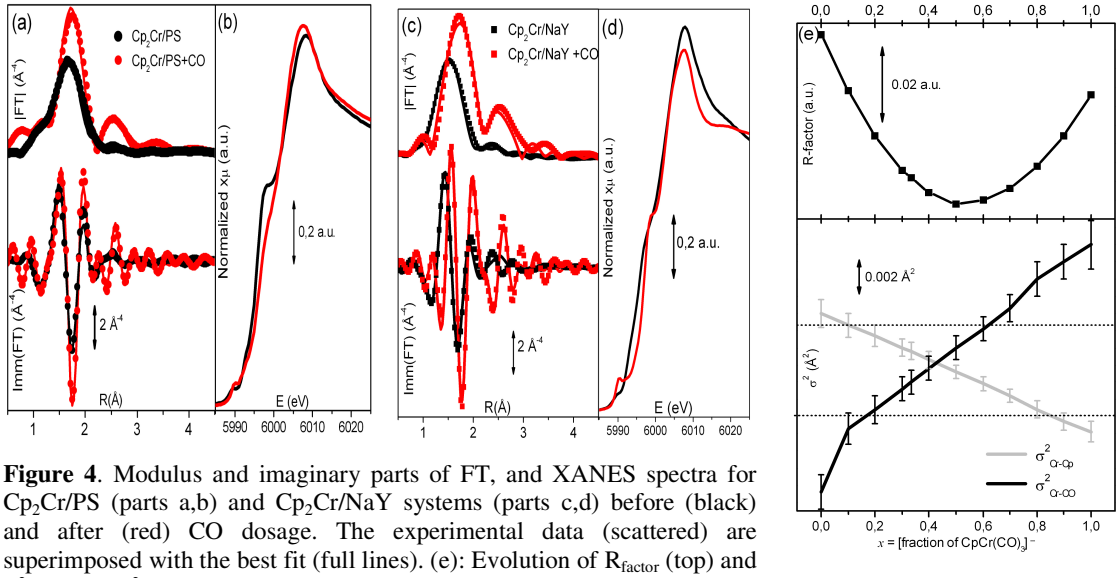

Figure 4. Modulus and imaginary parts of FT, and XANES spectra for Cp_2Cr/PS (parts a,b) and Cp_2Cr/NaY systems (parts c,d) before (black) and after (red) CO dosage. The experimental data (scattered) are superimposed with the best fit (full lines). (e): Evolution of R_{factor} (top) and $\sigma^2_{Cr\text{-}Cp}$ and $\sigma^2_{Cr\text{-}CO}$ (bottom) as a function of the fraction x of $[CpCr(CO)_3]^-$ species optimized in two-phases fits performed at fixed x values.

Table 2. Summary of the parameters optimized in the fit of the EXAFS data for the $Cp_2Cr/PS+CO$ and $Cp_2Cr/NaY+CO$ systems. The fits were performed in ΔR=1.0-4.5 Å range. Not optimized parameters have no error bars; optimized values

	$Cp_2Cr/PS+CO$	$Cp_2Cr/NaY+CO$			
	1 phase	1 phase	1 phase	2 phases	
	$Cp_2Cr(CO)$	$[CpCr(CO)_3]^-$	$[Cp_2Cr(CO)]^+$	$[CpCr(CO)_3]^-$	$[Cp_2Cr(CO)]^+$
S_0^2	0.7	0.9 ± 0.2	0.6 ± 0.1*	0.9·x	0.9·(1-x)
ΔE_0 (eV)	2 ± 2	1 ± 2	1 ± 2	3 ± 1	
$<d_{Cr\text{-}C}>$ (Å)	2.18 ± 0.01	2.193 ± 0.009	2.20 ± 0.01	2.227 ± 0.006	2.196 ± 0.006
$\sigma^2_{Cr\text{-}Cp}$ (Å^2)	0.0058 ± 0.0007	0.001± 0.001*	0.004 ± 0.002	0.0047 ± 0.0006	
$<d_{Cr\text{-}CO}>$ (Å)	1.87 ± 0.01	1.82 ± 0.02	1.85 ± 0.01	1.822 ± 0.006	1.893 ± 0.006
$\sigma^2_{Cr\text{-}CO}$ (Å^2)	0.003 ± 0.002	0.012 ± 0.002*	0.000 ± 0.001*	0.006 ± 0.001	
N variables	5	6	6	6	
R_{factor}	0.049	0.046	0.035	0.013	

The k^3-weighted FT of the EXAFS data are shown in Figure 4c. We initially performed two separate fits by supposing the presence of only one of the two species but both of them gave numerical results physically unreliable (values marked with stars in Table 2). Therefore we tried to quantitatively evaluate the relative amounts of the two species by means of a two phases fit. A phase fraction parameter x was added to the fit, weighting the signals of the species $[CpCr(CO)_3]^-$ and $[Cp_2Cr(CO)]^+$ by x and (1-x), respectively, see Figure 4e. Other parameters have been constrained in order to keep fixed the same number of variables optimized to 6, as for the two previous fits, so that they are directly comparable. The phase fraction parameter x was optimized to 0.50±0.07. This value was confirmed to

be an absolute minimum in a R-factor vs. *x* trend (Figure 4e). So that it is concluded that the two species are almost equi-populated.[18]

4. Conclusions

Both PS and NaY zeolite matrixes are able to molecularly isolate Cp_2Cr molecules, thus allowing the study of their interactions with simple reagents from the gas phase (operation that is much more difficult in the case of a liquid solution). The differences between the two matrixes in terms of polarity are reflected on the encaged molecules, slightly in terms of geometry, but especially in terms of their reactivity. In fact, interaction of Cp_2Cr with CO in PS gives a stable monocarbonyl complex, whereas in the zeolite a higher and more complex reactivity is observed, involving a Cp loss and the formation of $[CpCr(CO)_3]^-$ and $[Cp_2Cr(CO)]^+$ as final products.

References

(1) Ozin, G. A.; Gil, C. *Chem. Rev.* **1989**, *89*, 1749-1764.
(2) Stucky, G. D.; Macdougall, J. E. *Science* **1990**, *247*, 669-678.
(3) Sachtler, W. M. H.; Zhang, Z. C. *Adv. Catal.* **1993**, *39*, 129-220.
(4) Davis, M. E. *Nature* **2002**, *417*, 813-821.
(5) Kemner, E.; Overweg, A. R.; van Eijck, L.; Fitch, A. N.; Suard, E.; de Schepper, I. M.; Kearley, G. J. *J. Chem. Phys.* **2002**, *116*, 10838-10845.
(6) Kaiser, C. T.; Gubbens, P. C. M.; Kemner, E.; Overweg, A. R.; Jayasooriya, U. A.; Cottrell, S. P. *Chem. Phys. Lett.* **2003**, *381*, 292-297.
(7) Long, J. L.; Wang, X. X.; Zhang, G. Y.; Dong, J. G.; Yan, T. J.; Li, Z. H.; Fu, X. Z. *Chem.-Eur. J.* **2007**, *13*, 7890-7899.
(8) Karol, F. J.; Wu, C.; Reichel, W. T.; Marashin, N. J. **1979**.
(9) Green, J. C.; Jardine, C. N. *J. Chem. Soc.-Dalton Trans.* **1999**, 3767-3770.
(10) Salomon, O.; Reiher, M.; Hess, B. A. *J. Chem. Phys.* **2002**, *117*, 4729-4737.
(11) Xu, Z. F.; Xie, Y. M.; Feng, W. L.; Schaefer, H. F. *J. Phys. Chem. A* **2003**, *107*, 2716-2729.
(12) Poli, R.; Cacelli, I. *Eur. J. Inorg. Chem.* **2005**, 2324-2331.
(13) Swart, M. *Inorg. Chim. Acta* **2007**, *360*, 179-189.
(14) Chetwynd-Talbot, J.; Grebenik, P.; Perutz, R. N. *Inorg. Chem.* **1982**, *21*, 3641-3651.
(15) Tang Wong, K. L.; Brintzinger, H. H. *J. Am. Chem. Soc.* **1975**, *97*, 5143-5146.
(16) Brintzinger, H. H.; Lohr, L. L. J.; Tang Wong, K. L. *J. Am. Chem. Soc.* **1975**, *97*, 5146-5155.
(17) Estephane, J.; Groppo, E.; Vitillo, J. G.; Damin, A.; Lamberti, C.; Bordiga, S.; Zecchina, A. *Phys.Chem.Chem.Phys.* **2009**, *11*, 2218–2227.
(18) Estephane, J.; Groppo, E.; Damin, A.; Vitillo, J. G.; Gianolio, D.; Lamberti, C.; Bordiga, S.; Prestipino, C.; Nikitenko, S.; Quadrelli, E. A.; Taoufik, M.; Basset, J. M.; Zecchina, A. *J. Phys. Chem. C* **2009**, *113*, 7305–7315.
(19) Ravel, B.; Newville, M. *J. Synchrot. Radiat.* **2005**, *12*, 537-541.
(20) Ankudinov, A. L.; Ravel, B.; Rehr, J. J.; Conradson, S. D. *Phys. Rev. B* **1998**, *58*, 7565-7576.
(21) Ruiz-Lopez, M. F.; Loos, M.; Goulon, J.; Benfatto, M.; Natoli, C. R. *Chemical Physics* **1988**, *121*, 419-437.
(22) O'Callaghan, K. A. E.; Brown, S. J.; Page, J. A.; Baird, M. C. *Organometallics* **1991**, *10*, 3119-3122.
(23) Darensbourg, M. Y.; Jimenez, P.; Sackett, J. R.; Hanckel, J. M.; Kump, R. L. *J. Am. Chem. Soc.* **1982**, *104*, 1521-1530.
(24) Longato, B.; Martin, B. D.; Norton, J. R.; Anderson, O. P. *Inorg. Chem.* **1985**, *24*, 1389-1394.